Applied Catalysis B: Environmental 154–155 (2014) 153–160

Contents lists available at ScienceDirect

Applied Catalysis B: Environmental

journal homepage: www.elsevier.com/locate/apcatb

Effects of bismuth addition and photo-deposition of platinum on (surface) composition, morphology and visible light photocatalytic activity of sol–gel derived TiO_2

Wentao Yi[a,b,*], Chunyan Yan[a,b], Mohamed S. Hamdy[a,c], Jonas Baltrusaitis[a], Guido Mul[a,*]

[a] Photocatalytic Synthesis Group, Faculty of Science and Technology, MESA+ Institute for Nanotechnology, University of Twente, PO Box 217, 7500 AE Enschede, The Netherlands
[b] College of Chemistry, Chemical Engineering and Materials Science, Zaozhuang University, Zaozhuang 277160, China
[c] Chemistry Department, Faculty of Science, Helwan University, Cairo, Egypt

ARTICLE INFO

Article history:
Received 16 November 2013
Received in revised form 20 January 2014
Accepted 27 January 2014
Available online 3 February 2014

Keywords:
Platinum
Bismuth
Anatase
TiO_2
Photocatalysis
Water treatment

ABSTRACT

Several remarkable observations regarding structure, (surface) composition and visible light induced photocatalytic activity of Bi-promoted Anatase photocatalysts are reported. First, XPS characterization data show that compositions of mixed Bi-Ti-oxide phases obtained by hydrothermal treatment at 180 °C of aqueous solutions of ethanol, titanium n-butoxide, and bismuth nitrate, are surface enriched with a specific fraction of metallic-like bismuth. Second, the formation of highly dispersed nanoparticles of platinum on these composites by photo-deposition is accompanied by significant morphological changes. Third, the platinum functionalized, bismuth-promoted Anatase composites exhibit extraordinary photocatalytic activity in the photocatalytic degradation of organic compounds (acid orange 7 and salicylic acid, respectively) upon illumination at 447 nm, higher than observed for P25 upon UV illumination in similar reactor configuration. An optimized Pt-Bi-Ti-O_x composite consists of 1 wt% Pt and 5 wt% Bi. The high activity of the composite is discussed on the basis of the crystalline morphology and surface composition.

1. Introduction

Photocatalysis has been extensively studied in applications relevant for environmental remediation. In particular, TiO_2-based photocatalysts show high photocatalytic activity in conversion of dyes and toxins present in aqueous environment [1–4]. Unfortunately, ultraviolet irradiation (<387 nm) is needed to induce photo-excitation of TiO_2 [5]. In order to improve the light absorption properties of TiO_2, doping, or creation of composites constituting a so-called Z-scheme have been reported, and proven to be effective in increasing visible light photocatalytic activity [5–12]. While several combinations of oxides in semiconductor composites have been proposed, Bi_2O_3-TiO_2 composites have lately been demonstrated particularly effective in photo-oxidation processes [13–16]. Various synthesis procedures for the composites have been reported. However, the nature of the structure of the composites leading to the highest visible light sensitivity and inducing photocatalysis is not exactly known. Further, it has been reported that (surface) phases of Bi-oxides are very dynamic, depending on the experimental conditions [17]. Lastly, to the best of our knowledge, the effect of metal nanoparticles on photocatalytic activity of Bi_2O_3-TiO_2 composites has not been addressed in detail. Noble metal nanoparticles are known to promote electron transfer to adsorbed reactants in semiconductor based photocatalysis, thus resulting in higher rates [18,19].

In this contribution, we report on the photocatalytic behavior of bismuth titanate composites (Bi-Ti-O_x) with variable Bi/Ti ratio synthesized by a high temperature sol–gel method in the degradation of two model compounds representing toxins in an aqueous environment. We also investigated the effect of Pt to promote oxygen reduction. We will show a significant improvement in visible light performance of Bi-containing TiO_2 composites by addition of Pt nanoparticles prepared by photo-deposition. The catalytic performance is discussed on the basis of two remarkable observations: (i) the surface of the composites contains metallic-like Bi, and (ii) photo-deposition of Pt results in significant restructuring of the crystalline morphology and surface composition of the composites.

* Corresponding authors at: Faculty of Science and Technology, University of Twente, P.O. Box 217, 7500 AE Enschede, Netherlands. Tel.: +31 53 4893890; fax: +31 53 4892882.
E-mail addresses: wentaoyi@uzz.edu.cn (W. Yi), G.mul@utwente.nl (G. Mul).

0926-3373/$ – see front matter © 2014 Elsevier B.V. All rights reserved.
http://dx.doi.org/10.1016/j.apcatb.2014.01.055

2. Experimental

2.1. Materials and methods

All chemicals were purchased from Sigma–Aldrich and used without further purification. Bi-Ti-O_x was synthesized via a hydrothermal process. Typically, $Bi(NO_3)_3{\cdot}5H_2O$ was dissolved in a mixture of 2.0 mL 50% HNO_3, 5.0 mL deionized water and 10 mL ethanol to form solution A. In another flask, 10 mL titanium n-butoxide and 10 mL absolute ethanol were mixed homogeneously under magnetic stirring at room temperature to form solution B. Subsequently, solution A was added dropwise to solution B under vigorous stirring until a colorless homogeneous mixture was formed. The mixture was then transferred to a 100 mL Teflon-lined autoclave. The autoclave was heated at 180 °C for 15 h and cooled to room temperature. The product was collected by filtration, and washing with deionized water, and subsequently dried at 100 °C for 10 h. Finally, the product was calcined in air at 450 °C for 4 h (ramp rate 2 °C/min). The as prepared samples are labeled *y*-Bi-Ti-O_x, in which *y* refers to the % of Bi in the sample. For comparison, TiO_2 was also prepared by the above method, using solution A without dissolution of $Bi(NO_3)_3{\cdot}5H_2O$.

Pt promoted Bi-Ti-O_x was prepared by photo-deposition. A mixed solution of the required amount of Bi-Ti-O_x and H_2PtCl_6 was introduced to a batch, top illumination reactor and stirred in the dark for 1 h. Subsequently, methanol was added to obtain a concentration of 6% (volume percent). Then, the mixture was irradiated by using a high-pressure Hg lamp (Carl ZEISS, HBO 50 W) under magnetic stirring at 298 K for 10 h. The samples were collected by centrifuging the suspension, followed by washing with deionized water and absolute ethanol until no chloride anion could be detected in the filtrate by the AgCl deposition method. Subsequently the composite was dried at 100 °C for 6 h. For comparison, a Pt-TiO_2 sample was also prepared by the same procedure.

2.2. Characterization

The X-ray diffraction patterns (XRD) were recorded on a Bruker D2 X-ray diffractometer using Cu K_α radiation ($\lambda = 1.54056$ Å) operating at 30 kV and 10 mA over the 2θ range of 10–90°. The morphologies were characterized using a high resolution scanning electron microscope equipped with NORAN EDS and WDS (HR-SEM-LEO 1550) options. Raman spectra were obtained using a Bruker Senterra Raman Spectrometer equipped with a N_2 cooled CCD detector (213 K). Nitrogen adsorption measurements were carried out with a Micromeritics Tristar System ASAP 2400. Prior to adsorption measurements, the samples were degassed at 573 K and 10^{-3} Pa for 24 h, and the specific areas were calculated by the BET method. The diffuse reflectance UV-visible spectra (DRS) of the samples were recorded using an EVOLUTION 600 UV–vis spectrometer (Thermal Scientific), with a diffuse reflectance accessory at room temperature ($BaSO_4$ was used as reference). X-ray photoelectron spectroscopy (XPS) measurements were conducted using a Quantera SXM spectrometer (Physical Electronics), and the radiation was provided by a monochromatized Al Kα X-ray source (1486.6 eV) operated at a 50 W emission power and a 15 kV acceleration voltage. The binding energies were referenced to the C1s line at 284.8 eV from adventitious carbon. Energy-dispersive X-ray spectra (EDS) were recorded using a HR-SEM-LEO 1550 scanning electron microscope with an energy-dispersive attachment in order to investigate the surface chemical composition. The bulk composition of the materials was analyzed by X-ray fluorescence spectroscopy.

Table 1
Overview of the effect of pH on the degradation rate of AO7 and SA. (Conditions: 447 nm visible light, illumination for 120 min, AO7 concentration of 20 mg L^{-1}, SA of 40 mg L^{-1}, 5Bi-Ti-O_x concentration of 2 g L^{-1}, room temperature).

AO7	pH	2.2	3.5	5.4	6.8
	c/c_0	0.59	0.58	0.63	0.69
SA	pH	2.4	–	–	6.5
	c/c_0	0.59	–	–	0.67

2.3. Photocatalytic evaluation

The photocatalytic activity was tested using acid orange (AO7) and salicylic acid (SA) as model compounds in a home-made box reactor, which was equipped with a 12 V electronic fan to control the temperature and humidity, a multi-position magnetic stirrer (MIX 15 eco, Germany), and 8 independently controlled light tubes. The photocatalytic degradation was carried out in 100 mL glass containers with 20 mg L^{-1} aqueous AO7 solution or 40 mg L^{-1} SA solution in the presence of 2 g L^{-1} catalyst under magnetic stirring and air purging (25 mL min^{-1} per reactor). The slurries were stirred in the dark for 60 min to establish adsorption/desorption equilibrium. Then, the mixture was placed at a distance of 10 cm from the light sources (visible light: Philips violet 18 W tubes with λ maximizing at 447 nm; UV light: Philips TL-D 18 W tubes, with λ maximizing at 375 nm). For comparison, a blank experiment without catalyst was performed under the same conditions. Table 1 contains some preliminary data on degradation stages of the reagents (concentration of reagent after 120 min of reaction (C) over initial concentration (C_0)) at different pH values, demonstrating that acidic conditions are favoring conversion. Therefore catalyst comparison was conducted (at room temperature) by adjusting the pH of the AO7 solutions to 3.5, and of the SA solutions to 2.4. Adequate aliquots of the mixtures were taken at periodic intervals during irradiation, and after filtration by a 0.2 μm PTFE Milipore membrane filter, they were analyzed with an UV-visible spectrometer correlating a 485 nm absorption or 295 nm absorption with AO7 and SA concentrations, respectively. Per example, the time-dependent UV–vis spectra of AO7 degradation in an experiment using a 1Pt-5Bi-Ti-O_x photocatalyst exposed to visible light (447 nm), are shown in Fig. 1. Clearly, molecular absorption of the AO7 dye has disappeared after approximately 30 min of reaction.

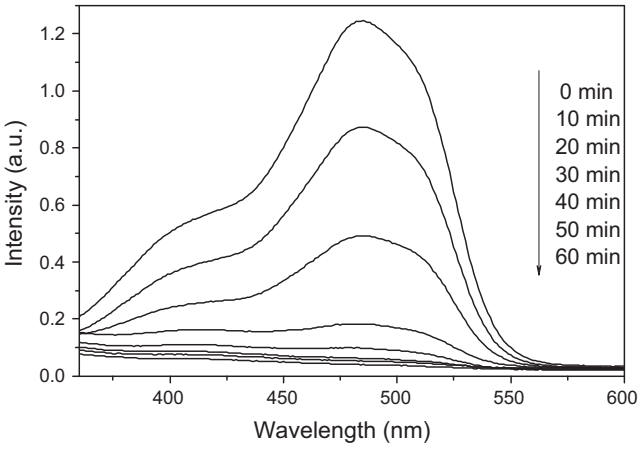

Fig. 1. Time-dependent UV–vis spectra of AO7 degradation in an experiment using the 1Pt-5Bi-Ti-O_x photocatalyst exposed to visible light (447 nm).

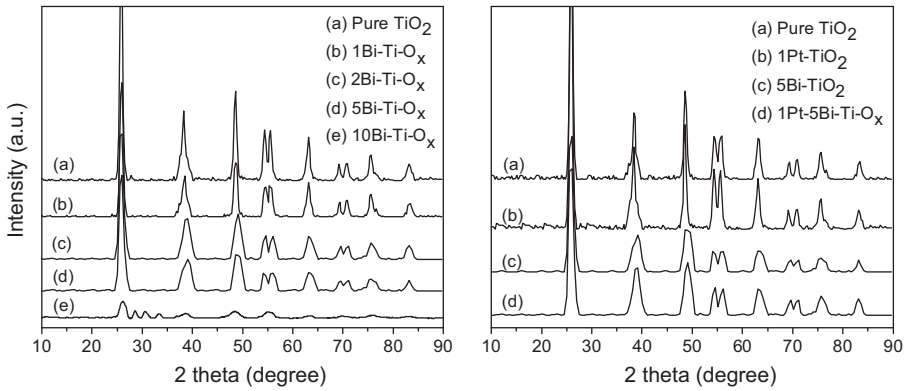

Fig. 2. XRD patterns of as-prepared samples (Left panel: TiO_2 doped with different amounts of Bi. Right panel: TiO_2, 1Pt-TiO_2, 5Bi-Ti-O_x and 1Pt-5Bi-Ti-O_x).

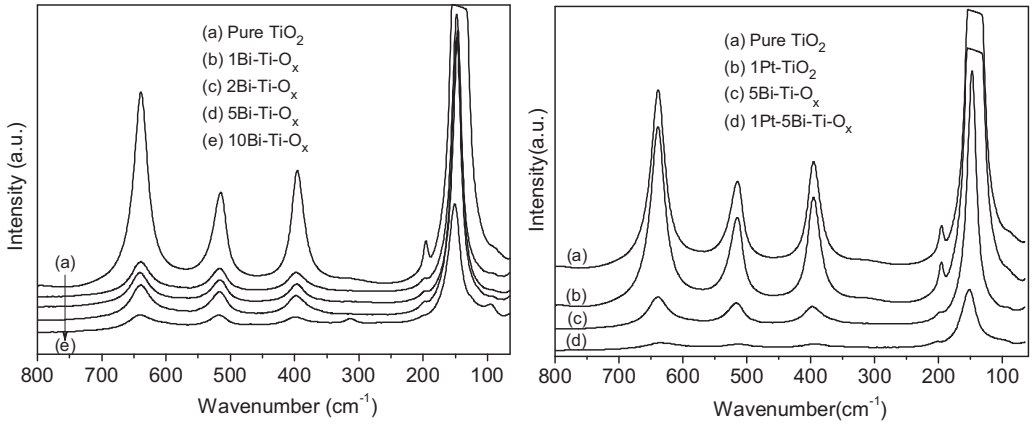

Fig. 3. Raman spectra of as-prepared samples (Left panel: TiO_2 doped with different amounts of Bi. Right panel: pure TiO_2, 1Pt-TiO_2, 5Bi-Ti-O_x and 1Pt-5Bi-Ti-O_x).

3. Results and discussion

3.1. Characterization

The crystal structure of the prepared samples was investigated by X-ray diffraction (XRD) and the patterns are presented in Fig. 2. All XRD patterns clearly show the main characteristic lines of Anatase, with the (1 0 1), (0 0 4), (2 0 0), (1 0 5), (2 1 1), (2 0 4), (1 1 6), (2 2 0), (2 1 5) and (3 1 2) signals showing up at 2θ values of ca. 25.4°, 37.8°, 47.9°, 53.9°, 55.2°, 62.6°, 68.8°, 70.8°, 75.6° and 83.2°, respectively (according to the American Society for Testing and Materials, standard no. 21-1272). Diffraction lines indicative of Bi_2O_3 phases were not observed in Bi-Ti-O_x and Pt-Bi-Ti-O_x samples, except when the Bi content is equal to 10 wt% (in 10Bi-Ti-O_x, lines at 2θ values of 30.8° and 33.6° correspond to Bi_2O_3, and the line at 28.5° to $Bi_4Ti_3O_{12}$ [20]).

The primary particle size of the composite nanoparticles is estimated to decrease as a function of increasing Bi content on the basis of the broadening of the anatase diffraction lines. This indicates that the presence of Bi^{3+} in the precursor solution inhibits the growth of anatase crystallites. In addition, it has been previously reported that the presence of Bi^{3+} in Titania composites prevents sintering during calcination at elevated temperatures [21], which can also explain the increase in line broadening upon addition of Bi up to 5 wt%, in agreement with the following Raman spectra presented in Fig. 3.

The major peaks located at 144, 196, 399, 519 and 639 cm^{-1} can be ascribed to the characteristic Raman bands of Anatase [22]. The intensity of the bands decreases gradually and the bands broaden as a function of increasing amount of Bi. This confirms the XRD data, in that the crystallinity of the bismuth doped samples decreases. The peaks at 103 and 315 cm^{-1} correspond to a monoclinic Bi_2O_3 phase [23], only apparent in sample 10Bi-Ti-O_x, again in agreement with the XRD results.

Fig. 4 shows the diffuse reflectance spectra of the prepared samples. The absorption at wavelengths shorter than 400 nm can be assigned to the intrinsic band-gap absorption of TiO_2. It is clear that the addition of Bi results in a stronger absorption in the visible light region. If Bi is introduced in the Anatase phase substitutionally or interstitually, we speculate this introduces new energetic states in the band gap of Anatase, explaining the observed changes in light

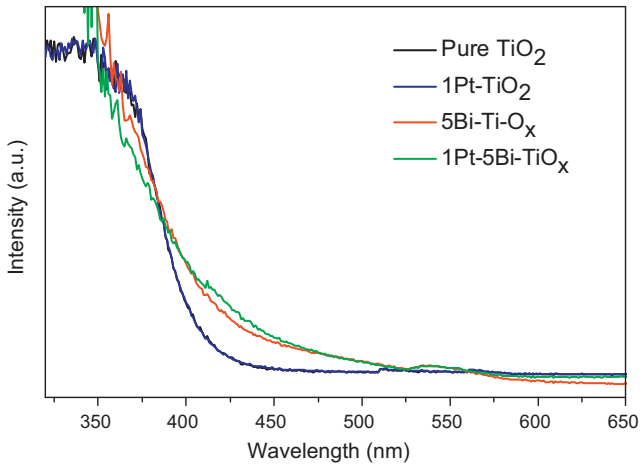

Fig. 4. UV–vis DR spectra of TiO_2, 1Pt-TiO_2, 5Bi-Ti-O_x and 1Pt-5Bi-Ti-O_x.

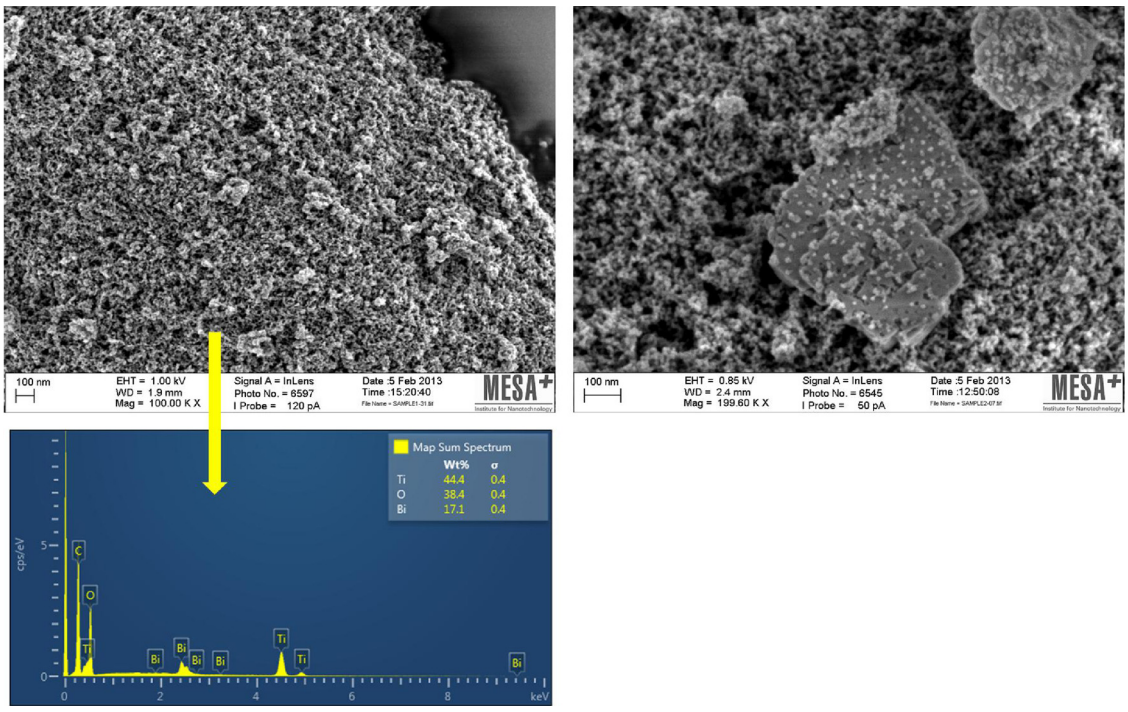

Fig. 5. HR-SEM micrographs of 5Bi-Ti-O_x (left panel) and 1Pt-5Bi-Ti-O_x (right panel) and corresponding EDS analyses (bottom).

absorption. Addition of Pt (see spectrum of Pt-Bi-Ti-O_x) results in an apparently even higher absorption intensity in the wavelength range centered at 425 nm, which we speculate to be related to additional absorptions of light by the Pt-(Bi) nanoparticles.

Fig. 5 shows the HR-SEM micrographs of the 5Bi-Ti-O_x (left panel) and 1Pt-5Bi-Ti-O_x (right panel) composites. It can be clearly seen that the sample before the photo-deposition of Pt exhibits a porous semi-crystalline morphology, without significant segregated crystalline matter. After photo-deposition of Pt, crystallization appears to have occurred to a much larger extent. This appears to be related to the presence of Bi, since these recrystallization phenomena have to the best of our knowledge not been previously reported for studies in which photo-deposition of Pt on pure Anatase phases was applied.

In order to study the elementary distribution of the different metals in the novel crystallites, EDS analysis was conducted, as shown in Fig. 6. Fig. 6 demonstrates a generally even distribution of all metals, although some areas of higher Bi and congruent Pt concentration appear to coincide with the small particulates observed in the HR SEM micrograph.

Fig. 7 shows the nitrogen adsorption–desorption isotherms and the corresponding BET areas before and after Pt photo-deposition. The 5Bi-Ti-O_x sample shows a hysteresis loop of type V, suggesting a mesoporous structure according to the IUPAC classification. Contrary, after Pt photo-deposition, 1Pt-5Bi-Ti-O_x shows a type III hysteresis loop in the p/p_0 range of 0.8–1.0. After calculation, a significant reduction from 14 to 1.5 m^2/g in BET surface area can be determined. Such dramatic decrease in surface area agrees with an increase in crystal size as discussed on the basis of the XRD analyses and SEM micrographs.

XPS analysis of 5%Bi-TiO_2 and 1%Pt-5%Bi-TiO_2 samples was performed to identify chemical species present on the surface of the composites. High resolution XPS spectra of the Ti2p, O1s, Bi4f and Pt4f regions are shown in Fig. 8. The $Ti2p_{3/2}$ peak at 459.2 eV can be assigned to Ti^{4+} species [24]. No other titanium oxidation states are observed. The presence of Ti^{4+} species is in agreement with a single peak observed at 530.1 eV in the O1s spectrum, typical for metal oxides [25,26]. Interestingly, only a minor quantity of adsorbed surface hydroxyl species can assigned to the O1s spectra, as can be inferred from a slight shoulder at 531.9 eV [26]. A Ti2p/O1s ratio of 1.83 was found, suggesting the surface to be slightly deficient of oxygen. The Bi4f region showed two doublet peaks with the corresponding $Bi4f_{7/2}$ maxima located at 156.9 and 159.5 eV, and the corresponding $Bi4f_{5/2}$ maxima located at 162.1 and 165.0 eV. These can be attributed to metallic Bi and Bi^{3+}, respectively [27], suggesting a partial reduction of surface Bi. The Bi^{3+} energy is higher than observed for pure α-Bi_2O_3 [28], and in agreement with a proposal for the formation of surface BiO(OH) [29]. Metallic Bi formation was observed in doped TiO_2 by others, but the formation thereof was not explained [30]. However, alcohols (glucose) have been reported previously to lead to reduction of precipitating Bi-compounds [31], and the presence of ethanol in combination with the high synthesis temperature (180 °C) might be the cause of this observation in the present study. Further, a peak of reduced Bi at a binding energy of 157.2 eV was observed in Bi-doped $NaTaO_3$ [32]. These authors proposed different chemical environments of Bi, possibly in locations of Na or Ta sites, to explain the presence of metallic Bi. We propose that the lower energy Bi peak is not necessarily entirely due to metallic Bi, but a phase containing reduced Bi near an O vacancy might also contribute to the Bi^0-like signal. It is known that O vacancies in Ti will possess unpaired electrons which will reduce nearby metal ions [33]. We argue that the much greater electron affinity of Bi will make it prone towards reduction by electrons present in oxygen vacancies of the TiO_2 lattice, as opposed to the low electron affinity of titanium atoms (0.942 vs. 0.079 eV, respectively) [34].

In the sample modified by Pt photo-deposition, the $Pt4f_{7/2}$ peak at 71.8 eV, and $Pt4f_{5/2}$ at 75.2 eV are very close to values reported in the literature for Pt^0 [35]. After deposition of Pt, the values of the $Bi4f_{7/2}$ and $Bi4f_{5/2}$ signals of reduced and oxidized phases of Bi show a different relative intensity as compared to the sample before Pt deposition: it appears as if some of the metallic-like Bi species have oxidized. Besides the intensity ratio, the peak positions have also shifted. The $Bi4f_{7/2}$ maxima are now located at 157.2 and 159.1 eV, and the corresponding $Bi4f_{5/2}$ maxima located

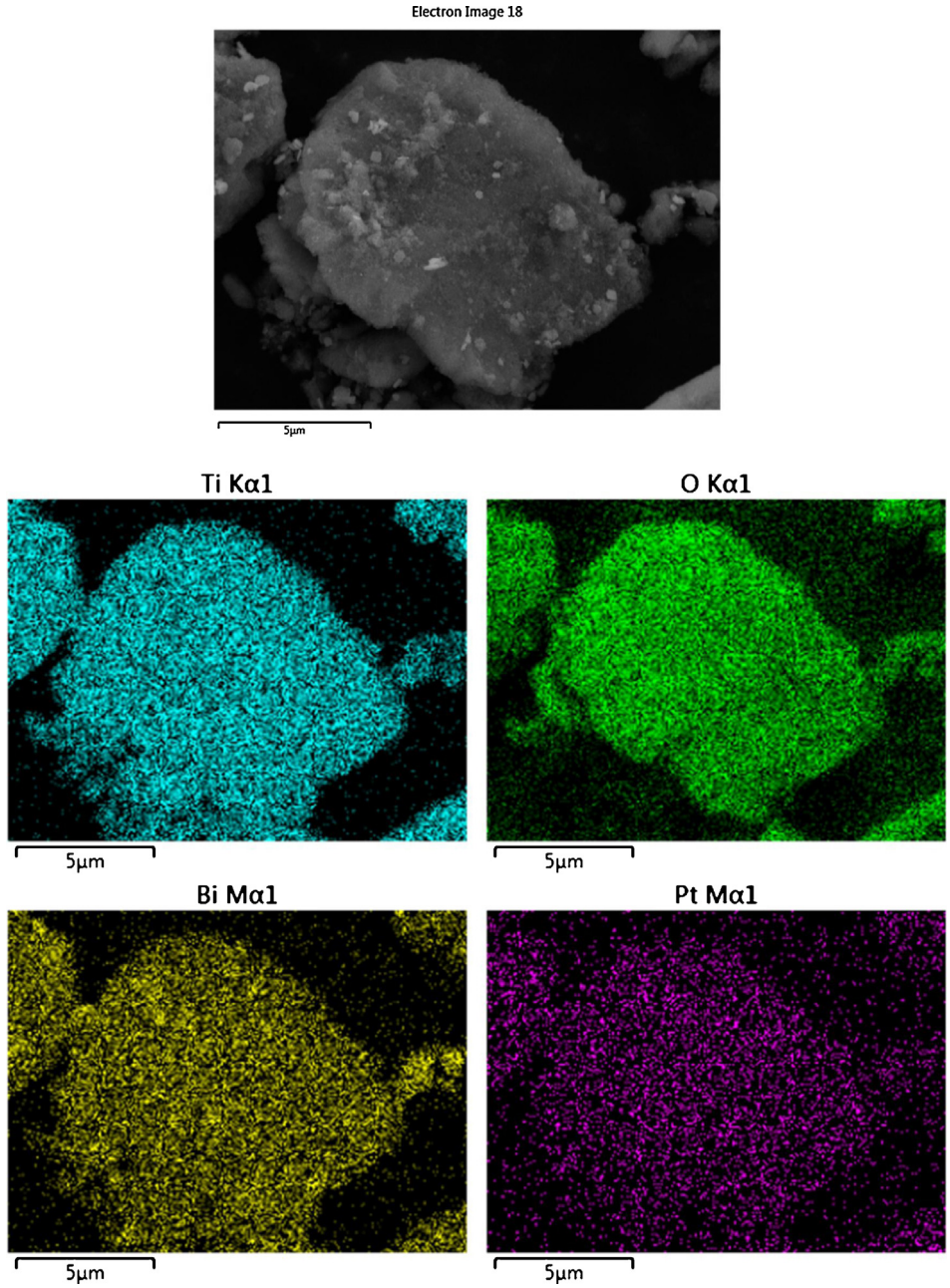

Fig. 6. HR-SEM micrographs of 1Pt-5Bi-Ti-O_x, including elemental distribution.

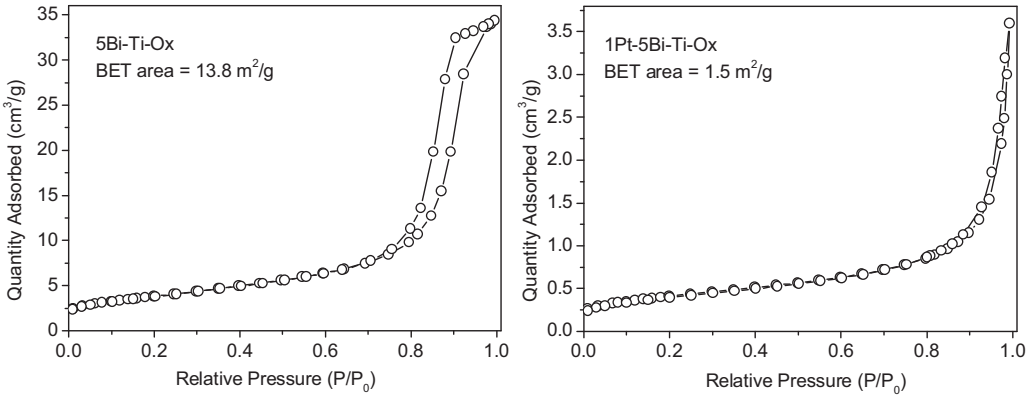

Fig. 7. Isotherms of 5Bi-Ti-O_x (Left panel) and 1Pt-5Bi-TiO_x (Right panel).

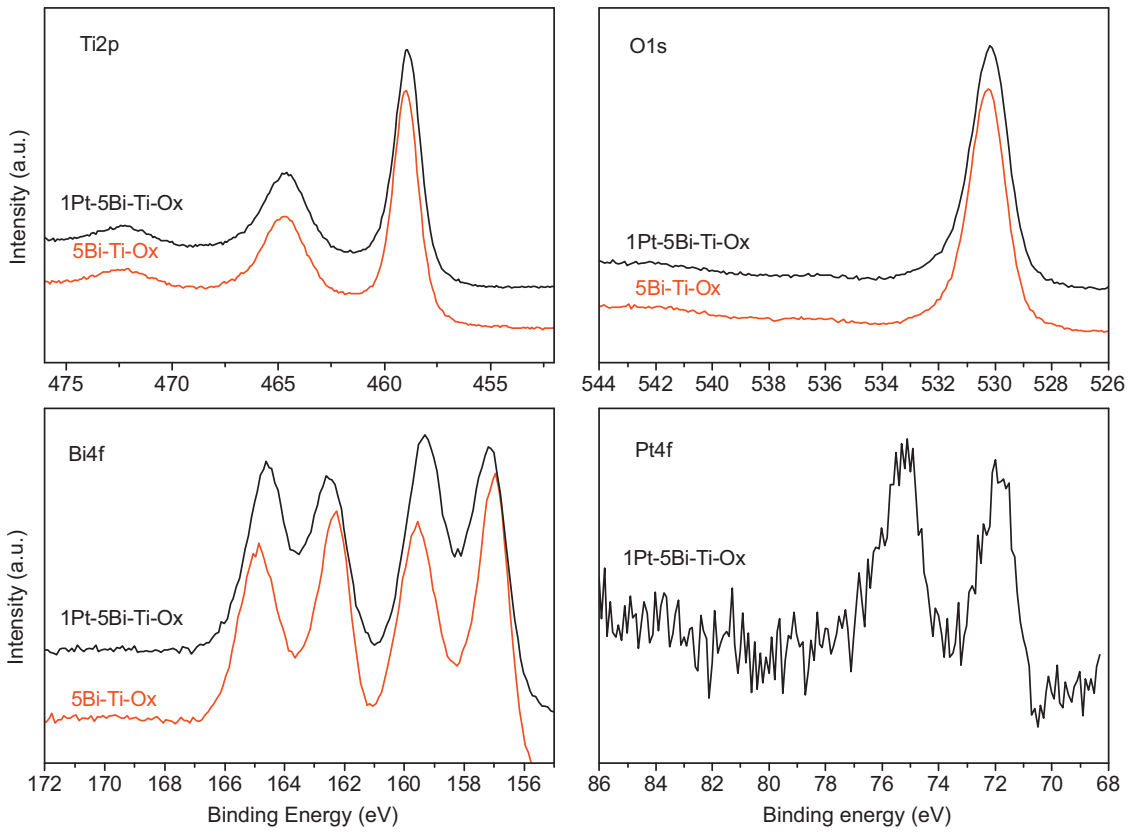

Fig. 8. XPS data of 5Bi-Ti-O_x and 1Pt-5Bi-Ti-O_x.

at 162.6 and 164.5 eV. The Bi^{3+} signals have thus shifted downward by ~0.5 eV, whereas the Bi^0 signals have shifted upward by ~0.5 eV. Although speculative, the following explanations might be considered. Regarding the upward shift of Bi^0, this might be related to Bi–Pt interactions. In Pt–Bi alloys, a value for Bi^0 at 157.2 eV has been reported [29]. These authors specifically state that the value of 157.2 eV is higher than observed for metallic Bi (ranging from 156.6 to 157.1), corroborating the assignment to Pt–Bi alloy like species. Regarding the downward shift of Bi^{3+}, we can speculate the BiO(OH) surface phase has been transferred to another phase, in agreement with the vast restructuring observed in the microscopy images. This is most likely related to the strongly acidic (HCl) conditions applied in the photo-deposition experiments. Restructuring of $BiVO_4$ upon acid treatment in HCl has recently been discovered to lead to dissolution of Bi^{3+} and recrystallization to BiOCl [36]. Further, downward shifts in Bi^{3+} signals have been recently reported for BiOCl catalysts when comparing the reported XPS data of the material before and after exposure to light in photocatalytic experiments [37]. A value for light exposed BiOCl has been reported at 159.2 eV [37]. Unfortunately, this shift is not described, nor discussed. In agreement with partial BiOCl formation, we have established a surface Bi:Cl ratio of 3:1 to be present in the sample after photo-deposition, by comparing Cl and Bi intensities in the XPS survey. In addition to oxychloride formation, the change in position of Bi^{3+} could be related to formation of higher oxides in the catalyst surface layer, indicated by $Bi_2O_{(4-x)}$, as proposed by Fornasiero and coworkers [17]. These phases have been discussed to be formed upon light exposure of Bi_2O_3, and reported to have improved photocatalytic properties. The shift in the XPS maxima of the Bi^{3+} signals to lower binding energies is then related to some oxygen vacancies in the vicinity. These have a well-known reductive behavior as they share their unpaired electron density with the metal atom. Concluding, we propose (light induced) inter-conversion of surface BiO(OH) to BiO(Cl) and possibly oxides of higher oxidation states to tentatively explain the change in Bi^{3+} position in the XPS spectra.

In summary, the characterization data suggest a composition of the composite before photo-deposition consisting of Bi-Ti-O_x, surface functionalized with BiO(OH), and a significant fraction of metallic-like Bi up to a loading of 5 wt%. At higher loading separate phases have been identified in Raman and XRD spectroscopy. After photo-deposition, metallic Pt is formed, possibly interacting with the reduced metallic-like Bi phase, while the BiO(OH) phase is most likely (partially) converted to BiOCl or $Bi_2O_{(4-x)}$ phases, tentatively proposed to explain the formation of large crystals. Irrespective of the mechanism, vast recrystallization of a significant fraction of the Bi-Ti-O_x composite is apparent from the loss in surface area and observation of crystalline matter in the SEM micrographs.

3.2. Photocatalytic activity evaluation of the samples

3.2.1. Effect of bismuth loading on the photocatalytic activity of composites

The apparent first order rate constants of the Bi-Ti-O_x composites in photocatalytic degradation of AO7 under visible light irradiation ($\lambda \sim 447$ nm) and UV light irradiation ($\lambda \sim 375$ nm) are compared in Fig. 9. The rate constants are significantly higher upon UV excitation for all samples as compared to visible light excitation, but the presence of Bi clearly induced visible light activity. The trend in activity as a function of increasing Bi content might be explained by a decrease in primary particle size of the samples up to 5 wt% Bi, as well as by favorable light absorption properties induced by increasing Bi concentrations. At even higher loading of Bi, segregated Bi oxide (containing) phases are formed, apparently leading to decreasing activity. Based on the light intensity entering the reactor, photonic efficiencies can be calculated to range from 1%

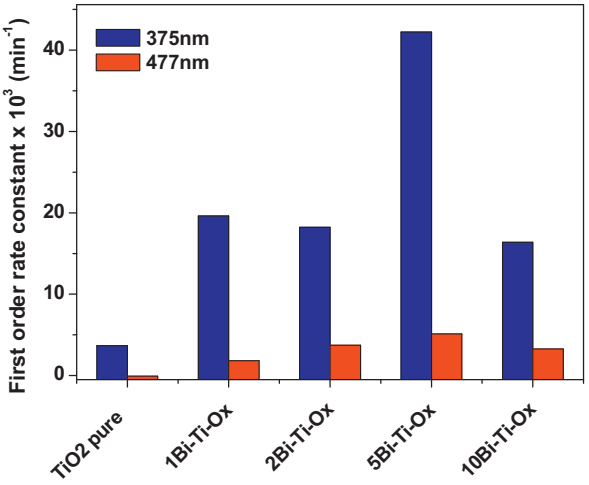

Fig. 9. First order photocatalytic rate constants in degradation of AO7 over various Bi-Ti-O_x catalysts upon UV light and visible light activation (conditions: AO7 concentration of 20 mg L^{-1}, pH of 3.5, photocatalyst concentration of 2 g L^{-1}, room temperature).

for TiO_2, to 5% for 5Bi-Ti-O_x. Because of the highest rate constant, 5Bi-Ti-O_x was selected for further investigation.

3.2.2. Effect of Pt addition

Photocatalytic degradation of AO7 and SA was performed over pure TiO_2, 1Pt-TiO_2, 5Bi-Ti-O_x, and 1Pt-5Bi-Ti-O_x under visible light illumination (447 nm) in order to quantify the positive effects of Pt and Bi on improving the photocatalytic performance of home-made TiO_2. As shown in Fig. 10, the blank experiment without catalyst indicates that photolysis of AO7 and SA can be neglected. Further, TiO_2 and 1Pt-TiO_2 are inactive since these catalysts do not absorb visible light, in good agreement with the DRS results. A significantly higher photocatalytic rate constant is obtained for 1Pt-5Bi-Ti-O_x as compared to 5Bi-Ti-O_x. The enhancement in activity is remarkably large, in particular considering the order of magnitude loss in specific surface area after the Pt deposition procedure. It is worth noting that AO7 seems much easier to be photocatalytically degraded than SA.

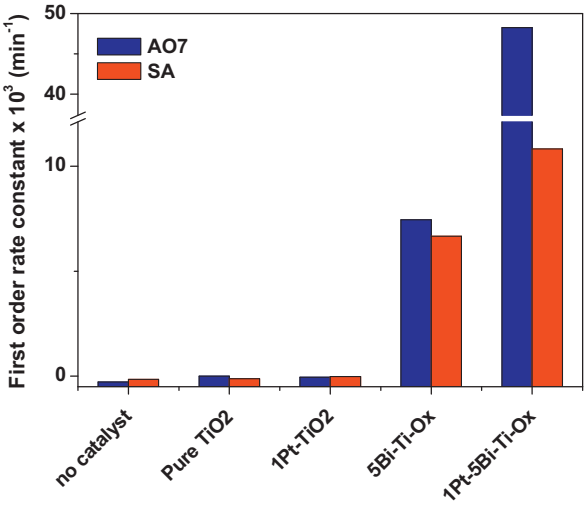

Fig. 10. First order photocatalytic rate constants in AO7 degradation (AO7 concentration 20 mg L^{-1}, pH of 3.5, photocatalyst concentration of 2 g L^{-1}, room temperature) and SA degradation (SA concentration of 40 mg L^{-1}, pH of 2.4, photocatalyst concentration of 2 g L^{-1}, room temperature) of TiO_2, 1Pt-TiO_2, 5Bi-Ti-O_x, and 1Pt-5Bi-Ti-O_x, respectively, under visible light illumination.

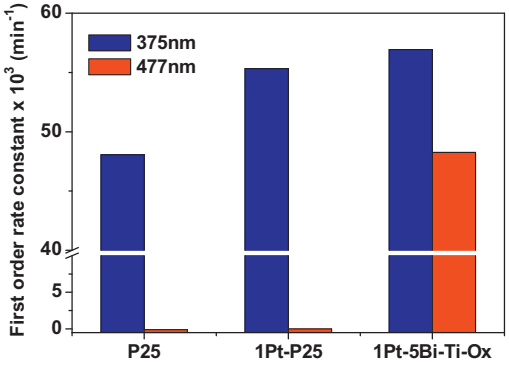

Fig. 11. Photocatalytic rate constants of P25, 1Pt-P25 and 1Pt-5Bi-Ti-O_x (conditions: AO7 concentration of 20 mg L^{-1}, pH of 3.5, photocatalyst concentration of 2 g L^{-1}, room temperature).

3.2.3. Photocatalytic activity comparison of 1Pt-5Bi-Ti-O_x with 1Pt-P25

To further position the excellent performance of the 1Pt-5Bi-Ti-O_x composite, a comparison with P25 and Pt/P25 for degradation of AO7 both under UV light and visible light is shown in Fig. 11. As expected, P25 and Pt/P25 are inactive under visible light illumination. The addition of Pt to P25 (TiO_2) leads to an increase in decomposition rate constant upon UV light activation, although not dramatically. Clearly, 1Pt-5Bi-Ti-O_x shows superior photocatalytic activity under visible light activation, while the activity of the composite is somewhat enhanced by changing Visible light for UV. In the comparison with P25, also the large difference in surface area should be considered. Whereas the overall BET area of P25 is typically 55 m^2/g, the composite only provides 1.5 m^2/g.

In summary, the novel composite 1Pt-5Bi-Ti-O_x is significantly more active under visible light illumination, than Pt/P25 under UV light illumination, when corrected for surface area.

3.2.4. Recycle test of 1Pt-5Bi-Ti-O_x

Stability of photocatalysts is one of the key factors determining practical feasibility of heterogeneous photocatalysis technology. The stability of the 1Pt-5Bi-Ti-O_x was studied in the degradation of AO7 under visible-light irradiation (447 nm). After four cycles, the 1Pt-5Bi-Ti-O_x catalyst does not exhibit significant loss of activity, as shown in Fig. 12, confirming that the components of 1Pt-5Bi-Ti-O_x are not photo-corrosive, and that the structure is relatively stable in reaction conditions of photocatalysis.

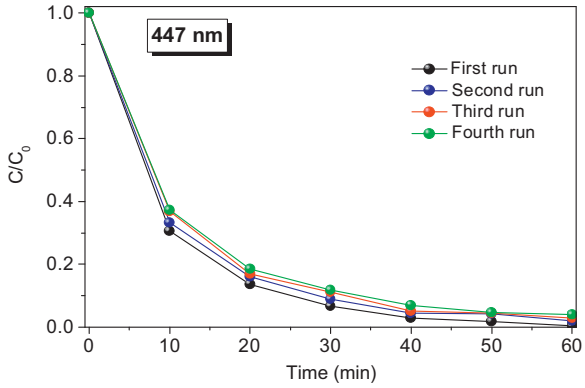

Fig. 12. Stability evaluation of 1Pt-5Bi-Ti-O_x (conditions: AO7 concentration of 20 mg L^{-1}, pH of 3.5, photocatalyst concentration of 2 g L^{-1}, room temperature).

3.2.5. Proposed structure–activity correlation

Bi_2O_3 and TiO_2 combinations have been studied in photocatalytic applications by several researchers [14–16]. Usually Bi_2O_3 is deposited on pre-existing titania phases. Then, a high photocatalytic activity upon visible light excitation is typically explained by transfer of photo-excited states (electrons and holes) between phases. In the present study, a high temperature one pot sol–gel procedure in the presence of ethanol is used to synthesize the composites. Since the rate constant for the composite of the highest Bi loading (10 wt%), consisting of oxidic bismuth containing phases in addition to Anatase, is significantly lower as compared to the optimized loading of 5 wt%, charge transfer between phases is less likely to explain the high activity in the present study. Rather we speculate that Bi^{3+} has been incorporated in the Anatase phase either substitutionally or interstitially, leading to Bi^{3+} associated energetic states within the band gap of Anatase. These states provide for the visible light absorption and photocatalytic activity of the material. The observed activity might be enhanced by (i) the presence of surface BiO(OH), providing hydroxyl radicals upon excitation, and/or (ii) metallic Bi, stimulating oxygen reduction, but this is rather speculative.

As shown by the photocatalytic data, the activity of the composite has dramatically improved after applying the Pt photodeposition procedure. At the same time the microscopy, and N_2 sorption data suggest a significant crystal restructuring and reduction in surface area, making the enhancement in activity even more remarkable. Obviously, noble metal nanoparticles are known to promote electron transfer to adsorbed reactants in semiconductor based photocatalysis, thus resulting in higher rates [18,19], and certainly the presence of the Pt nanoparticles will contribute to the enhanced activity. In the present study Pt likely promotes the oxygen reduction reaction. In addition, XPS data provide some leads to further explain the enhancement. First, it appears as if metallic Bi is interacting with the deposited Pt phase, which could lead to a synergy in promoting oxygen reduction. This obviously requires further investigation, comparing enhancement in activity by Pt/Bi alloy nanoparticles to Pt nanoparticles. Further, although not conclusive, it appears restructuring of the Bi (surface) morphology has taken place, which likely has generated photocatalytically more effective Bi phases. As stated in explaining the XPS data, both a (surface) BiOCl phase could have been formed, as well as novel active oxidic states. The potentially present surface BiOCl compound could constitute an electron transfer scheme with Bi-doped anatase phases, which might reduce electron–hole (excited state) recombination [11,12]. The novel Bi oxide phases might intrinsically have high reactivity, contributing to the remarkable activity observed [17].

Finally the difference in rates observed for AO7 decomposition and SA decomposition require some discussion. This may be related to different photocatalytic mechanisms. Absorption of visible photons by the dye AO7 might contribute to its degradation [38]. It has been previously observed that Bi based catalysts show very effective rates in Methyl Orange degradation [17], which is presumably the consequence of photo-excitation of the dye, and subsequent photocatalytic degradation reactions.

4. Conclusions

A one-step hydrothermal synthesis procedure was applied to prepare photoactive samples of bismuth-promoted Anatase. An unexpected metallic Bi phase was apparent on the surface of the composite. The prepared samples exhibit visible light induced photocatalytic activity in AO7 and SA oxidation. An optimized Bi-Ti-O_x composite consists of 5 wt% Bi. Higher Bi quantities lead to phase segregation (Bi_2O_3 and bismuth titanate are formed) and loss in activity. Photo-deposition of 1 wt% Pt enhances the photocatalytic performance dramatically, despite recrystallization and loss in surface area induced by the photo-deposition procedure. The platinized sample seems to be a very promising photocatalyst under visible light illumination. The synergy between the various components in this intriguing catalyst requires further investigation, in particular the possible formation and effectiveness of Pt/Bi nanoparticles to promote photocatalysis.

Acknowledgments

W. Yi and C. Yan were financially supported by the Science and Technology Research Program of Shandong Province, China (No.hj008). The authors would like to thank J.S. Romão for N_2 sorption measurements, R. Amrollahi for Raman spectroscopy, M. Smithers for the HRSEM analysis, and G. Kip for the XPS analysis.

References

[1] A. Fujishima, K. Honda, Nature 238 (1972) 37–38.
[2] X. Chen, L. Liu, P.Y. Yu, S.S. Mao, Science 331 (2011) 746–750.
[3] K. Elghniji, J. Soro, S. Rossignol, M. Ksibi, J. Taiwan Inst. Chem. E. 43 (2012) 132–139.
[4] A.A. Hebeish, M.M. Abdelhady, A.M. Youssef, Carbohydr. Polym. 91 (2013) 549–559.
[5] D.M. Tobaldi, R.C. Pullar, A.F. Gualtieri, M.P. Seabra, J.A. Labrincha, Chem. Eng. J. 214 (2013) 364–375.
[6] W.K. Ho, J.C. Yu, S.C. Lee, J. Solid State Chem. 179 (2006) 1171–1176.
[7] K. Uboncholakate, L. Sikong, F. Saito, Procedia Eng. (Elsevier) 32 (2012) 656–662.
[8] Y.M. Wu, M.Y. Xing, J.L. Zhang, J. Hazard. Mater. 192 (2011) 368–373.
[9] A. Fuerte, M.D. Hernandez-Alonso, A.J. Maira, A. Martinez-Arias, M. Fernandez-Garcia, J.C. Conesa, J. Soria, Chem. Commun. 37 (2001) 2718–2719.
[10] S. Murcia López, M.C. Hidalgo, J.A. Navío, G. Colón, J. Hazard. Mater. 185 (2011) 1425–1434.
[11] H. Hua, Y. Xi, Z. Zhao, X. Xie, C. Hu, H. Liu, Mater. Lett. 91 (2013) 81–83.
[12] J.J. Xu, Y.H. Ao, D.G. Fu, C.W. Yuan, Appl. Surf. Sci. 255 (2008) 2365–2369.
[13] Y. Hu, Y. Cao, P. Wang, D. Li, W. Chen, Y. He, X. Fu, Y. Shao, Y. Zheng, Appl. Catal. B Environ. 125 (2012) 294–303.
[14] X. Zhao, H.J. Liu, J.H. Qu, Appl. Surf. Sci. 257 (2011) 4621–4624.
[15] Z. Bian, J. Zhu, S. Wang, Y. Cao, X. Qian, H. Li, J. Phys. Chem. C 112 (2008) 6258–6262.
[16] K. Su, Z.H. Ai, L.Z. Zhang, J. Phys. Chem. C 116 (2012) 17118–17123.
[17] A. Hameed, T. Montini, V. Gombac, P. Fornasiero, J. Am. Chem. Soc. 130 (2008) 9658–9659.
[18] R.P. Antony, T. Mathews, C. Ramesh, N. Murugesan, A. Dasgupta, S. Dhara, S. Dash, A.K. Tyagi, Int. J. Hydrogen Energy 37 (2012) 8268–8276.
[19] X. Hu, H. Ji, L. Wu, RSC Adv. 2 (2012) 12378–12383.
[20] B.D. Stojanović, C.O. Paiva-Santos, M. Cilense, Č Jovalekić, Z.Ž. Lazarević, Mater. Res. Bull. 43 (2008) 1743–1753.
[21] X. Zhu, Z. Liu, J. Fang, S. Wu, W. Xu, J. Mater. Res. 28 (2013) 1334–1342.
[22] H.C. Choi, Y.M. Jung, S.B. Kim, Vib. Spectrosc. 37 (2005) 33–38.
[23] M. Vila, C. Díaz-Guerra, J. Piqueras, Mater. Chem. Phys. 133 (2012) 559–564.
[24] C. Moreno-Castilla, F.J. Maldonado-Hódar, F. Carrasco-Marín, E. Rodríguez-Castellón, Langmuir 18 (2002) 2295–2299.
[25] J. Baltrusaitis, P.M. Jayaweera, V.H. Grassian, J. Phys. Chem. C 115 (2010) 492–500.
[26] J. Baltrusaitis, D.M. Cwiertny, V.H. Grassian, Phys. Chem. Chem. Phys. 9 (2007) 5542–5554.
[27] V.S. Dharmadhikari, S.R. Sainkar, S. Badrinarayan, A. Goswami, J. Electron. Spectrosc. Relat. Phenom. 25 (1982) 181–189.
[28] D. Barreca, F. Morazzoni, G.A. Rizzi, R. Scotti, E. Tondello, Phys. Chem. Chem. Phys. 3 (2001) 1743–1749.
[29] A.V. Tripković, K.Dj. Popović, R.M. Stevanović, R. Socha, A. Kowal, Electrochem. Commun. 8 (2006) 1492–1498.
[30] J. Ma, J. Chu, L. Qiang, J. Xue, RSC Adv. 2 (2012) 3753–3758.
[31] X. Liu, H. Cao, J. Yin, Nano Res. 4 (2011) 470–482.
[32] P. Kanhere, J. Zheng, Z. Chen, J. Phys. Chem. C 115 (2011) 11846–11853.
[33] X. Pan, M. Yang, X. Fu, N. Zhang, Y. Xu, Nanoscale 5 (2013) 3601–3614.
[34] R.C. Weast (Ed.), CRC Handbook of Chemistry and Physics, 93rd ed., CRC Press, Boca Raton, FL, 2013, 2012–2013.
[35] H.S. Kibombo, C.M. Wu, J. Baltrusaitis, R.T. Koodali, Appl. Catal. B Environ. 136–137 (2013) 248–259.
[36] M. Long, L. Wan, C. Zeng, Y. Liu, Y. Chen, Acta Physico-Chim. Sinica 28 (2012) 2917–2923.
[37] Z.Y. Yu, D. Bahnemann, R. Dillert, S. Lin, L.Q. Lu, J. Mol. Catal. A: Chem. 365 (2012) 1–7.
[38] C. Chen, W. Ma, J. Zhao, Chem. Soc. Rev. 39 (2010) 4206–4219.